The difference in immunohistochemical reactivity of monoclonal antibodies against amino-terminal residues of amyloid-β peptide

Short title: Differential immunohistochemical reactivity of anti-Aβ antibodies

Kana Araki[1, 2], Kenta Yamauchi[1, 2*], Shogo Ito[1, 2], Masato Koike[1] and Hioki Hiroyuki[1, 2, 3*]

[1]Department of Neuroanatomy, Juntendo University Graduate School of Medicine, Bunkyo-Ku, Tokyo, Japan

[2]Department of Cell Biology and Neuroscience, Juntendo University Graduate School of Medicine, Bunkyo-Ku, Tokyo, Japan

[3]Department of Multi-Scale Brain Structure Imaging, Juntendo University Graduate School of Medicine, Bunkyo-Ku, Tokyo, Japan

*Corresponding Authors

E-mail: ke-yamauchi@juntendo.ac.jp (KY) and h-hioki@juntendo.ac.jp (HH)

Author contributions

Conceptualization, K.A., K.Y. and S.I.; Methodology, K.A., K.Y. and S.I.; Investigation, K.A., K.Y., S.I. and H.H.; Formal Analysis, K.A., K.Y. and S.I.; Writing – Original Draft, K.Y.; Writing – Review & Editing, K.A., K.Y., S.I., M.K. and H.H.; Visualization, K.A., and K.Y.; Project Administration, K.Y.; Funding Acquisition, K.Y., S.I., M.K. and H.H..

Abstract

Immunohistochemistry for amyloid-β (Aβ) peptide is an indispensable method for Alzheimer's disease (AD) research. Despite a wide variety of available antibodies against the peptides, the difference of immunohistochemical reactivity is not fully described among anti-Aβ antibodies. Immunohistochemical reactivity of Abs against Aβ peptides is critical for accurate and reliable evaluation of Aβ burden in patients as well as models of AD. Here, we examined immunohistochemical reactivity of two mouse and one rabbit monoclonal antibodies against Aβ N-terminal regions using two AD mouse models, $App^{NL\text{-}F}$ and $App^{NL\text{-}G\text{-}F}$. 6E10, 82E1 and D54D2 Aβ antibodies were used in this study. We found significant differences in the immunohistochemical reactivity in both $App^{NL\text{-}F}$ and $App^{NL\text{-}G\text{-}F}$ models. While 6E10 immunoreactivity was mainly localized to Aβ plaques, D54D2 and 82E1 antibodies stained much more broadly beyond plaques. Interestingly, the latter two Abs showed blurred filamentous immunoreactivity beyond amyloid plaque cores. Double immunostaining using a tyramide signal amplification method, Fluorochromized Tyramide-Glucose Oxidase (FT-GO), suggested that the differential immunohistochemical outcomes were only partially attributable to their sensitivity. Moreover, heat induced epitope retrieval (HIER) did not affect the differential immunohistochemical outcomes. Our analysis indicates that outcomes of Aβ immunohistochemistry highly depends on the antibody used in the study.

Introduction

A major histopathological hallmark of Alzheimer's disease (AD) is deposition of amyloid-β (Aβ) peptides in the brain (1). Aβ peptide is produced through proteolytic processing of a transmembrane protein, amyloid precursor protein (APP) (2, 3). While β-secretase cuts on the N-terminal end of the Aβ peptide, γ-secretase cleaves APP protein at multiple sites at the C-terminal ends to give rise to heterogeneous Aβ species. Aβ peptide is highly fibrillogenic and aggregates into higher-order species such as oligomers, protofibrils, fibrils and plaques, which have detrimental effects on brain integrity (2, 3). More than 30 mutations in APP gene have been reported to cause familial Alzheimer's disease (FAD) (4). Aβ pathology precedes the clinical onset of dementia by over 20 years (5). These findings support the amyloid cascade hypothesis positing that deposition of Aβ plaques in the brain triggers a cascade of events that leads to neurodegeneration (6, 7). The recent successes of Aβ-immunotherapy trials further strengthen the hypothesis (8).

Among multiple Aβ imaging techniques, immunohistochemistry (IHC) with antibodies (Abs) against Aβ peptides is superior in sensitivity and specificity (9) and widely used for measuring Aβ load in AD patients as well as models. Microscopic examination of IHC staining for Aβ peptides is further utilized for the definitive diagnosis and neuropathological staging of AD in postmortem brains (9, 10). Various kinds of Abs against Aβ peptides have been developed over the past decades and adapted for IHC analysis (11-16). They show differences in clonality, host species, target amino acid sequences and modification. However, there is no consensus on which Abs should be used for the detection of Aβ peptide by IHC. Critically, the difference in IHC reactivity among anti-Aβ Abs are not fully described. The differential IHC reactivity of the Abs should affect neuropathologic analysis of Aβ deposition by IHC staining.

Here, we examined IHC reactivity of two mouse monoclonal and one rabbit monoclonal Abs against N-terminal residues of human Aβ peptides using two *App* knock-in (KI) mouse models. These Abs showed significant differences in both mouse models regarding IHC outcomes. We further asked

66 whether the differences could be attributable to their sensitivity and antigen masking.

Materials and Methods

Animals

This study was carried out in strict accordance with Fundamental Guidelines for Proper Conduct of Animal Experiments by the Science Council of Japan (2006). All animal procedures were conducted in compliance with ARRIVE (Animal Research: Reporting *In Vivo* Experiments) guidelines. The protocol was approved by the Institutional Animal Care and Use Committees of Juntendo University (Approval No. 2023194). All surgery was performed under sodium pentobarbital anesthesia, and all efforts were made to minimize suffering.

Male $App^{NL\text{-}G\text{-}F/NL\text{-}G\text{-}F}$ (17) mice (RBRC06344, RIKEN BioResource Research Center) at 14 months old were used. The mice were housed in 12/12 h light/dark cycle at 20–25 °C under specific pathogen-free conditions and given access to food and water ad libitum. Mice were euthanized if they reached the humane endpoints: self-mutilation, breathing problems/cyanosis or inability to access food or water. Animal health and behavior were monitored twice a week. Three randomly selected mice were subjected to immunohistochemical examination.

Tissue preparation

Anesthesia was induced by intraperitoneal injection of an overdose of sodium pentobarbital (200 mg/kg; P0776, Tokyo Chemical Industry) in accordance with American Veterinary Medical Association (AVMA) Guidelines for the Euthanasia of Animals (2020). Following assessment of adequate depth of anesthesia by eye-blink reflexes and toe-pinch withdrawal, the thorax was opened and the right atrium was cut to allow drainage. The heart was perfused with 20 mL of ice-cold phosphate-buffered saline (PBS), followed by 20 mL of ice-cold 4% paraformaldehyde (1.04005.1000, Merck Millipore) in 0.1 M phosphate buffer (PB; pH 7.4). Brains were removed from the skull, postfixed in the same fixative overnight and cryoprotected in 30% sucrose in 0.1 M PB at 4 °C. Fixed

91 brains of male *App*$^{NL\text{-}F/NL\text{-}F}$ (17) mice (RBRC06343, RIKEN BioResource Research Center) at 14
92 months old were provided by Dr. A. Miyawaki (RIKEN Center for Brain Science). The brains were
93 mounted on a freezing microtome (REM-710; Yamato Kohki Industrial) and cut into 30-μm-thick
94 coronal sections (18).
95

96 # IHC staining

97 IHC was performed by a free-floating method at 20–25 °C (19). The primary and secondary
98 Abs used are listed in S1 and S2 Tables respectively. Abs and streptavidin were diluted in 0.3% Triton
99 X-100 in PBS (PBS-X) containing 0.12% λ-carrageenan (035-09693; Sigma-Aldrich) and 1% normal
100 donkey serum (S30-100ML, Merck Millipore). Heat induced epitope retrieval (HIER) was
101 accomplished by overnight incubation at 60 °C in a citrate buffer (ab93678, abcam) prior to IHC
102 staining. Brain sections immunostained for Aβ were mounted onto glass slides (Superfrost micro slide
103 glass APS-coated, Matsunami Glass) and coverslipped with Fluoromount/Plus™ (K048, Diagnostic
104 Biosystems).

105 For single IHC staining with anti-Aβ Abs, brain sections were washed twice for 10 min in
106 PBS-X and reacted overnight with primary Abs. The sections were washed twice for 10 min in PBS-
107 X and reacted for 2 h with secondary Abs. After washing twice for 10 min in PBS-X, the sections were
108 incubated with PBS-X containing FSB (10 or 20 μg/mL, F308, Dojindo) and NeuroTrace 530/615 Red
109 Fluorescent Nissl Stain (1:100, N21482, Thermo Fisher Scientific), and washed twice for 10 min in
110 PBS-X.

111 For double IHC staining with 6E10 and 82E1 or D54D2 Aβ Abs, brain sections were reacted
112 first with 6E10 Ab, and then with biotinylated 82E1 or D54D2 Abs. In double IHC with 6E10 and
113 82E1 mouse monoclonal Abs, Alexa Fluor (AF) 488-conjugated Fab fragments of goat ant-mouse
114 IgG1 Ab (8.0 μg/mL) was applied prior to incubation with the biotinylated 82E1 Ab. AF 568-
115 conjugated streptavidin (2 μg/mL, S11226, Thermo Fisher Scientific) was used for the detection of the

116 biotinylated anti-Aβ Ab. In double IHC with 6E10 and D54D2 Aβ Abs, secondary Abs were
117 simultaneously applied following incubation with D54D2 Ab. After IHC staining, brain sections were
118 stained with FSB as above.

119 Fluorochromized Tyramide-Glucose Oxidase (FT-GO) immunofluorescence (IF) was
120 adapted for sensitive detection of 6E10 Aβ Ab (19). Following incubation for 30 min in PBS
121 containing 1% hydrogen peroxide, brain sections were washed twice for 10 min in PBS-X and reacted
122 overnight with biotinylated 6E10 Ab. The sections were washed twice for 10 min PBS-X, incubated
123 for 2 h in avidin-biotin complex solution (1:500, PK-6100, Vectastain Elite ABC kit, Vector
124 Laboratories), and washed twice for 10 min in PBS-X and twice for 5 min in 0.1 M PB. Then, the
125 sections were incubated for 10 min with an FT-GO reaction mixture which contained 10 μM CF568
126 tyramide (92173, Biotium). FT-GO reaction was initiated by adding β-D-glucose (16804-32, Nacalai
127 Tesque) into the mixture at 2 mg/mL and proceeded for 30 min. Following two washes in PBS-X for
128 10 min each, the sections were reacted overnight with a complex of 82E1 Ab (1.0 μg/mL) and AF 488-
129 conjugated Fab fragments of goat ant-mouse IgG1 Ab (1.0 μg/mL) and washed twice for 10 min in
130 PBS-X. The primary and secondary Ab complex was prepared following the manufacturer instruction.
131 In the indirect detection compared with FT-GO signal amplification, unconjugated 6E10 Ab and
132 Rhodamine Red X-conjugated Fab fragments of goat ant-mouse IgG1 Ab were used as primary and
133 secondary Abs, respectively. Brain sections were reacted with these Abs prior to incubation with 82E1
134 Ab.

135

136 Image acquisition and processing

137 Images were captured with a confocal laser scanning microscope (TCS SP8; Leica
138 Microsystem). A 16× multi-immersion (HC FLUOTAR 16x/0.60 IMM CORR VISIR, NA = 0.60,
139 Leica Microsystems) and 25× water-immersion (HC FLUOTAR L 25x/0.95 W VISIR, NA = 0.95,
140 Leica Microsystems) objective lenses were used. The confocal pinhole was adjusted to 1.0 or 2.0 Airy

141 unit. Z-stack images were collected at 1.5 to 8.0 μm intervals at 512×512 or 1,024×1,024 pixel
142 resolutions. Captured images were stitched and processed to create maximum intensity projection
143 images using Leica Application Suite X software (LAS X, ver. 3.5.5.19976, Leica Microsystems). The
144 brightness and contrast of images were adjusted using Fiji software (20) (ver. 2.14.0/1.54 f).
145

146 # Quantification

147 To assess IHC reactivity of 6E10, 82E1 and D54D2 Aβ Abs, immunohistochemically stained
148 area (IHCSA) of each Ab was measured in the cerebral cortex and hippocampus using Fiji software.
149 After subtracting background noise, the number of pixels above a threshold was counted and
150 designated as the IHCSA. The threshold was set manually for each image. The IHCSA was normalized
151 to the FSB-stained area, a proxy for Aβ load in each brain section. In the cerebral cortex, the IHCSA
152 was analyzed in the region which is located medial to the outer edge of CA3 pyramidal cell layer and
153 lateral to the inner edge of the dentate gyrus (DG) granule cell layer. The hippocampus was analyzed
154 in its entirety. For direct comparisons of staining properties between 6E10 and 82E1 or D54D2 Aβ
155 Abs, FSB-labeled plaques were randomly selected from the cerebral cortex of $App^{NL\text{-}F/NL\text{-}F}$ mice.
156 To assess effects of signal amplification resulting from FT-GO IF and antigen unmasking
157 with HIER, IHCSA of 6E10 or 82E1 Aβ Abs was measured and quantified in the cerebral cortex of
158 $App^{NL\text{-}F/NL\text{-}F}$ mice as above. The coverage area of 82E1 IHCSA by 6E10 IHCSA was calculated using
159 Fiji software. The region medial to the outer edge of CA3 pyramidal cell layer and lateral to the inner
160 edge of the DG granule cell layer was subjected to analysis.
161

162 # Statistical analysis

163 Statistical analyses were conducted using GraphPad Prism 9 software (Version 9.4.1 (458),
164 GraphPad Software). For comparisons among independent groups, Brown-Forsythe and Welch one-
165 way analysis of variance (ANOVA) followed by Tukey-Kramer post hoc test ($App^{NL\text{-}G\text{-}F/NL\text{-}G\text{-}F}$ mouse

166 hippocampus) or Kruskal-Wallis test followed by Dunn's post hoc test (*App*$^{NL\text{-}F/NL\text{-}F}$ mouse cerebral
167 cortex and hippocampus, and *App*$^{NL\text{-}G\text{-}F/NL\text{-}G\text{-}F}$ mouse cerebral cortex) were used. Wilcoxon test was
168 used for paired comparisons between groups (Direct comparisons between 6E10 and 82E1 or D54D2
169 Abs). For comparisons between two independent groups with a normal distribution, unpaired t test was
170 used (FT-GO signal amplification and antigen unmasking using HIER). All tests were two-sided.
171 Statistical significance was set at $P < 0.05$. Graphed data are represented as means ± standard
172 deviations (SDs).

173 IHCSA of 6E10, 82E1 and D54D2 Aβ Abs were examined in seven to nine sections from
174 three *App*$^{NL\text{-}F/NL\text{-}F}$ and *App*$^{NL\text{-}G\text{-}F/NL\text{-}G\text{-}F}$ mice. Thirty plaques in nine brain sections from three *App*$^{NL\text{-}}$
175 $^{F/NL\text{-}F}$ mice were used for direct comparisons between 6E10 and 82E1 or D54D2 Aβ Abs. Nine sections
176 from three *App*$^{NL\text{-}F/NL\text{-}F}$ mice were used to evaluate signal enhancement in 6E10 FT-GO IF and antigen
177 unmasking using HIER. The exact values of n are stated in the corresponding figure legends. Unusual
178 outliers were not found in the datasets.

179

180 Data availability

181 The datasets generated during and/or analyzed during the current study and all biological
182 materials reported in this article are available from the corresponding authors on reasonable request.

Results

Differential IHC reactivity of N-terminal Aβ Abs

We examined IHC reactivity of monoclonal Abs (mAbs) against N-terminal regions of human Aβ peptide, because 1) N-terminal Aβ Abs are assumed to detect total Aβ peptide in the specimen, 2) diversity of Aβ species generated by γ-secretase cleavage affects IHC outcomes using anti-Aβ Abs against the C-terminal residues (13) and 3) FAD mutations located at the middle of the Aβ sequence can alter binding properties of anti-Aβ Abs that react the region(17). The Aβ Abs studied were 6E10 (21), 82E1 (22) and D54D2 Aβ monoclonal Abs, which all were generated by immunization with N-terminal residues of Aβ peptide and commercially available. Table 1 summarizes host animals, isotypes, immunogens, epitopes and suppliers of these anti-Aβ Abs.

Table 1. Aβ Ab information used in this study

Clone name	Host/Isotype	Immunogen	Epitope	Manufacturer, Cat. No.	RRID
6E10(21)	Mouse/IgG1	Human Aβ 1-16 peptide	Aβ 3–8 peptide	BioLegend, 80301	AB_2565328
82E1(22)	Mouse/IgG1	Human Aβ 1-16 peptide	N-terminus end (Aβ 1–5 peptide)(22)	Immuno-Biological Laboratories, 10323	AB_1630806
D54D2	Rabbit/IgG	Near N-terminus of human Aβ peptide	Not determined	Cell Signaling Technology, 8243S	AB_2797642

We first compared IHC reactivity of these three Abs in *App*$^{NL\text{-}G\text{-}F}$ mouse model (17) (Fig. 1a). Aβ IHC using 6E10, 82E1 and D54D2 Aβ Abs was carried out in frozen brain sections of *App*$^{NL\text{-}G\text{-}F/NL\text{-}G\text{-}F}$ mice. These brain sections were further stained with a Congo-red derivative, 1-Fluoro-2,5-bis(3-carboxy-4-hydroxystyryl)benzene (FSB) (23), to assess Aβ deposition in each brain section. IHC reactivity for Aβ peptides was quite different among 6E10, 82E1 and D54D2 Abs (Fig. 1a). While moderate and scattered immunoreactivity was found in brain sections stained with 6E10 Ab (Fig. 1a$_1$),

202 82E1 and D54D2 Abs labeled more massively and intensely brain sections of *App*$^{NL\text{-}G\text{-}F/NL\text{-}G\text{-}F}$ mice
203 (Fig. 1a$_{2,3}$). IHC reactivity were similar between 82E1 and D54D2 Aβ Abs. The same tendency was
204 found in *App*$^{NL\text{-}F/NL\text{-}F}$ mouse models (Fig. 1b), where Aβ burden is much less severe than *App*$^{NL\text{-}G\text{-}F/NL\text{-}}$
205 $^{G\text{-}F}$ mice (17). IHCSA normalized to Aβ fibril deposition assessed by FSB labeling was measured and
206 quantified in the cerebral cortex and hippocampus of both models (Fig. 1c, d). IHCSA of 82E1 and
207 D54D2 Aβ Abs was 2.49 to 4.49 times broader than that of 6E10 Aβ Ab. There were no significant
208 differences in IHCSA between 82E1 and D54D2 Abs (Fig. 1c, d). Additionally, the significant
209 difference in IHCSA was not detected between 6E10 and 82E1 Abs in the hippocampus of *App*$^{NL\text{-}F/NL\text{-}}$
210 ^{F} mice.
211
212 **Fig 1. Differential IHC reactivity among 6E10, 82E1 and D54D2 Aβ Abs.**
213 **a, b**) Aβ IHC in *App*$^{NL\text{-}G\text{-}F/NL\text{-}G\text{-}F}$ (**a**) and *App*$^{NL\text{-}F/NL\text{-}F}$ (**b**) mouse brain sections. 6E10 (**a$_1$, b$_1$**), 82E1 (**a$_2$,**
214 **b$_2$**) and D54D2 (**a$_3$, b$_3$**) Aβ Abs are used for the IHC. **c, d**) Histograms showing The IHCSA of 6E10,
215 82E1 and D54D2 Abs in *App*$^{NL\text{-}G\text{-}F/NL\text{-}G\text{-}F}$ (**c**) and *App*$^{NL\text{-}F/NL\text{-}F}$ (**d**) mice. The IHCSA in the cerebral
216 cortex (left) and hippocampus (right) are represented (*App*$^{NL\text{-}G\text{-}F/NL\text{-}G\text{-}F}$: n = 7 sections, 6E10 Ab in the
217 Ctx; n = 7 sections, 82E1 Ab in the Ctx; n = 9 sections, D54D2 Ab in the Ctx from 3 animals; H =
218 14.59, df = 2, P = 0.0009, Kruskal-Wallis test; n = 8 sections, 6E10 Ab in the Hipp; n = 9 sections,
219 82E1 Ab in the Hipp; n = 9 sections, D54D2 Ab in the Hipp from 3 animals; F = 35.42, df = 2, P <
220 0.0001, Brown-Forsythe ANOVA test. *App*$^{NL\text{-}F/NL\text{-}F}$: n = 8 sections, 6E10 Ab in the Ctx; n = 8 sections,
221 82E1 Ab in the Ctx; n = 9 sections, D54D2 Ab in the Ctx from 3 animals; H = 11.88, df = 2, P = 0.0026,
222 Kruskal-Wallis test; n = 9 sections, 6E10 Ab in the Hipp; n = 9 sections, 82E1 Ab in the Hipp; n = 9
223 sections, D54D2 Ab in the Hipp from 3 animals; H = 13.91, df = 2, P = 0.001, Kruskal-Wallis test).
224 Data are represented as means ± SDs. Ctx: cerebral cortex, Hipp: hippocampus, Thl: Thalamus. Scale
225 bar: 1000 μm. *P < 0.05; **P < 0.01; ***P < 0.001; ****P < 0.0001.
226

227 We then directly compared IHC reactivity of the anti-Aβ Abs by double IHC staining (Fig.
228 2). We analyzed IHC reactivity in the cerebral cortex of *App*$^{NL\text{-}F/NL\text{-}F}$ mice, because massive Aβ plaque
229 burden in *App*$^{NL\text{-}G\text{-}F/NL\text{-}G\text{-}F}$ mice makes it difficult to examine staining properties of these Abs in detail
230 (Fig. 1a). Given that 82E1 and D54D2 Abs showed comparable IHC reactivity (Fig. 1c, d), IHC
231 reactivity was compared between 6E10 and 82E1 or D54D2 N-terminal Aβ Abs. For this, we
232 conducted sequential double IHC staining. Following incubation of 6E10 Ab, 82E1 or D54D2 Ab was
233 applied to brain sections to prevent the latter two Abs from preoccupying the epitope of 6E10 Ab.
234 Again, 82E1 and D54D2 Abs showed much stronger IHC reactivity than 6E10 Ab in the direct
235 comparison (Fig. 2a, b). Of all analyzed plaques, 82E1 and D54D2 Abs stained broader regions than
236 6E10 Ab did (Fig. 2c, d). IHCSA of 82E1 and D54D2 Abs was 2.67 and 4.25 times broader
237 respectively than that of 6E10 Ab (Fig. 2c, d). Whereas 6E10 immunoreactivity was mainly localized
238 to plaque cores, 82E1 and D54D2 Abs stained much broader regions over amyloid cores visualized by
239 FSB labeling (Fig. 2a, b). Interestingly, 82E1 and D54D2 Abs showed blurred filamentous
240 immunoreactivity beyond plaque cores (Fig. 2a, b). 6E10 IHCSA narrower than the FSB-stained area
241 was found in approximately half of analyzed plaques (33 plaques in 60 plaques).
242
243 **Fig 2. Direct comparisons of IHC characteristics between 6E10 and 82E1 or D54D2 Aβ Abs.**
244 **a, b**) Double IHC with 6E10 and 82E1 (**a**) or D54D2 (**b**) Aβ Abs in the cerebral cortex of *App*$^{NL\text{-}F/NL\text{-}}$
245 ^{F} mice. FSB is used for labeling Aβ fibrils. $\mathbf{a_{1\text{-}4}}$, $\mathbf{b_{1\text{-}4}}$) Representative images for 6E10 Ab (yellow, $\mathbf{a_1}$,
246 $\mathbf{b_2}$), 82E1 (magenta, $\mathbf{a_2}$) or D54D2 Ab (magenta, $\mathbf{b_2}$) and FSB (cyan, $\mathbf{a_3}$, $\mathbf{b_3}$) staining. $\mathbf{a_4}$, $\mathbf{b_4}$) Merged
247 images of ($\mathbf{a_1}$), ($\mathbf{a_2}$) and ($\mathbf{a_3}$), and ($\mathbf{b_1}$), ($\mathbf{b_2}$) and ($\mathbf{b_3}$), respectively. **c, d**) Direct comparisons of IHCSA
248 of 6E10 and 82E1 (**c**) or D54D2 Aβ Abs (**d**) (n = 30 plaques from 9 sections of 3 animals for each;
249 6E10 vs 82E1 Abs: $W = 465.0$, $df = 1$, $P < 0.0001$, Wilcoxon matched-pairs signed rank test; 6E10 vs
250 D54D2 Abs: $W = 465.0$, $df = 1$, $P < 0.0001$, Wilcoxon matched-pairs signed rank test). Data are
251 represented as means ± SDs. Scale bar: 30 μm. ****$P < 0.0001$.

252

253 One possible explanation for the differential IHC outcomes among 6E10, 82E1 and D54D2
254 N-terminal Aβ Abs is the difference of IHC sensitivity of these Abs. If differential IHC sensitivity
255 underlies the differential outcomes of IHC, signal amplification techniques that enhances IHC
256 sensitivity should close the gap of IHC reactivity among Abs. We thus conducted FT-GO IF for 6E10
257 Ab and compared IHC reactivity of 82E1 Ab. FT-GO is a fluorescent tyramide signal amplification
258 system (TSA) technique, yielding 10- to 30-fold signal amplification compared with indirect IHC
259 detection (19). Because the epitope of D54D2 Ab has not been described in detail (Table 1), this Ab
260 was excluded from the analysis. Even after signal amplification by FT-GO, IHCSA of 82E1 Ab was
261 still much broader than that of 6E10 Ab (6E10/82E1^{+} IHCSA in 82E1^{+} IHCSA [means ± SDs]: FT-
262 GO, 0.442 ± 0.081) (Fig. 3). FT-GO signal amplification actually enhanced IHC sensitivity of 6E10
263 Ab: IHCSA of FT-GO detection was significantly broader than that of indirect detection (Fig. 3c)
264 (6E10/82E1^{+} IHCSA in 82E1^{+} IHCSA [means ± SDs]: indirect method, 0.318 ± 0.079; FT-GO, 0.442
265 ± 0.081, P = 0.0046, unpaired t test). These results imply that the difference of IHC sensitivity is only
266 partially attributable to the differential IHC outcomes between 6E10 and 82E1 Abs. We further
267 examined antigen masking effects on the differential IHC reactivity. Antigen retrieval techniques such
268 as HIER is frequently used for Aβ IHC staining to unmask epitopes. However, an HIER procedure did
269 not affect differential IHC outcomes between 6E10 and 82E1 Abs (Fig. 4). The gap of IHC reactivity
270 between 6E10 and 82E1 Abs still remained in brain sections treated with HIER (Fig. 4c) (6E10/82E1^{+}
271 IHCSA in 82E1^{+} IHCSA [means ± SDs]: wo/HIER, 0.362 ± 0.087; w/ HIER, 0.407 ± 0.073, P =
272 0.2454, unpaired t test).

273

274 **Fig 3. Signal amplification characteristics of 6E10 Aβ Ab by FT-GO.**

275 **a, b**) Double IHC with 6E10 and 82E1 Aβ Abs in the cerebral cortex of *App*$^{NL\text{-}F/NL\text{-}F}$ mice. 6E10 (**a**)
276 and Biotin-6E10 Ab (**b**) are detected with an indirect method (**a**) and FT-GO signal amplification (**b**),

respectively. 82E1 Ab is labeled with an AF 488 conjugated FabuLight antibody prior to incubation with brain sections. **a_{1-3}, b_{1-3}**) Representative images for 6E10 Ab (yellow, **a_1, b_1**) and 82E1 Ab (magenta, **a_2, b_2**) staining. **a_3, b_3**) Merged images of (**a_1**) and (**a_2**), and (**b_1**) and (**b_2**), respectively. **c**) Histograms representing the proportion of 82E1 IHCSA covered by 6E10 IHCSA (n = 9 sections from 3 animals for each; t = 3.288, df = 16, P = 0.0046, unpaired t test). Data are represented as means ± SDs. Scale bar: 50 μm.

Fig 4. The effect of antigen unmasking on the differential IHC reactivity between 6E10 and 82E1 Aβ Abs.

a, b) Double IHC with 6E10 and 82E1 Aβ Abs in the cerebral cortex of $App^{NL\text{-}F/NL\text{-}F}$ mice. Double Aβ IHC is performed in non-treated (**a**) and HIER-treated (**b**) brain sections. **a_{1-3}, b_{1-3}**) Representative images for 6E10 Ab (yellow, **a_1, b_1**) and 82E1 Ab (magenta, **a_2, b_2**) staining. **a_3, b_3**) Merged images of (**a_1**) and (**a_2**), and (**b_1**) and (**b_2**), respectively. **c**) Histograms representing the proportion of 82E1 IHCSA covered by 6E10 IHCSA (n = 9 sections from 3 animals for each; t = 1.206, df = 16, P = 0.2454, unpaired t test). Data are represented as means ± SDs. Scale bar: 50 μm.

292 # Discussion

293 In the present study, we analyzed IHC characteristics of two mouse and one rabbit monoclonal
294 Abs against N-terminal regions of Aβ peptide that recognize several isoforms of Aβ peptide and
295 transgenically expressed human APP. We found significant differences of IHC reactivity among these
296 Abs in both $App^{NL\text{-}F}$ and $App^{NL\text{-}G\text{-}F}$ mouse models: while 6E10 immunosignal was mainly localized to
297 plaque cores labeled by FSB, 82E1 and D54D2 Abs stained much more broadly beyond cores. Our
298 results further implied that the differential IHC outcomes between 6E10 and 82E1 Abs was only
299 partially attributable to IHC sensitivity of these Abs by using a fluorescent TSA system, FT-GO.
300 Antigen unmasking with a HIER technique did not affect the difference of IHC reactivity between
301 6E10 and 82E1 Abs.

302 6E10, 82E1 and D54D2 N-terminal Aβ Abs showed significant differences regarding their
303 IHC characteristics, even despite similarities in their prepared immunogens. These Aβ Abs are widely
304 assumed and used to detect total Aβ peptides. IHCSA of 82E1 and D54D2 Abs was much broader than
305 that of 6E10 Ab (Fig. 1). In contrast to immunoreactivity of 6E10 Ab, which was mainly localized to
306 amyloid cores, 82E1 and D54D2 Abs showed blurred filamentous immunosignals beyond plaque cores
307 in addition to immunoreactivity against core region (Fig. 2). The IHC reactivity against filamentous
308 materials around plaque cores can account for the broader IHCSA of 82E1 and D54D2 Abs. The
309 blurred filamentous immunoreactivity might reflect the deposition of protofibrillar and/or fibrillar
310 forms of Aβ peptides onto the brain (2, 3). Our finding that the coverage area of 82E1 IHCSA by 6E10
311 immunosignals was increased by FT-GO signal amplification indicates that differential IHC sensitivity
312 between 6E10 and 82E1 Abs partially explains their differential IHC outcomes (Fig. 3c). However,
313 the differential IHC sensitivity does not account for most of the difference of IHC reactivity between
314 these two Aβ Abs, because a substantial portion of 82E1 IHCSA was still not covered by 6E10
315 immunosignal even after FT-GO signal amplification (Fig. 3b). Our finding that an HIER procedure
316 failed to fill the gap of IHC reactivity between 6E10 and 82E1 Abs argues against the view that antigen

317 masking effects of formaldehyde fixation causes the differential IHC reactivity between the two Aβ
318 Abs (Fig. 4). The slight difference of epitopes within N-terminal regions of Aβ peptide between 6E10
319 and 82E1 Aβ Abs (Table 1) might generate and/or lose affinities for specific forms of the peptides in
320 frozen brain sections. While the epitope of 6E10 Ab lies within amino acids 3-8 of Aβ peptide, 82E1
321 Ab is an N-terminus end specific antibody (22). We cannot rule out the possibility that stronger signal
322 amplification than FT-GO close the gap completely between 6E10 and 82E1 IHCSA.

323 We found differential IHC characteristics of anti-Aβ Abs in both $App^{NL\text{-}G\text{--}F}$ and $App^{NL\text{-}F}$
324 mouse models (Fig. 1). $App^{NL\text{-}G\text{-}F}$ model which harbors Swedish (KM670/671NL), Beyreuther/Iberian
325 (I716F) and Arctic (E693G) mutations is being used most frequently as it develops Aβ pathology much
326 faster than other *App* knock-in lines (24). Aβ sequence of $App^{NL\text{-}F}$ model, which carries the Swedish
327 and Beyreuther/Iberian mutations, is identical to that of wild-type human (17). We consider that our
328 findings of significant differences of IHC characteristics among 6E10, 82E1 and D54D2 Abs could be
329 extrapolatable to other mouse models of AD which express APP FAD mutants transgenically, because
330 the most commonly used mutations in these FAD mutant models are the Swedish and/or
331 Beyreuther/Iberian mutations that are carried by $App^{NL\text{-}G\text{-}F}$ and $App^{NL\text{-}F}$ mouse models (25). Notably,
332 Aβ42 filament structure in $App^{NL\text{-}F}$ model are identical to type II filaments from human brains (26).
333 Further studies are required to determine whether the difference of IHC reactivity among Aβ Abs is
334 also found in the brain of AD patients.
335

336 Conclusions

337 A wide variety of anti-Aβ Abs developed over the past decades make the knowledge about
338 IHC reactivity of Abs against Aβ peptides important for accurate and reliable evaluation of Aβ plaque
339 burden in patients as well as models of AD. Our results demonstrate that Aβ IHC outcomes highly
340 depend on what kind of Ab is used for the analysis. This could be of importance for meta-analysis

341 where the results of Aβ IHC staining using various kinds of Abs are pooled.

342 # Acknowledgements

343 We thank Drs. Hiroshi Hama (RIKEN Center for Brain Science) and Atsushi Miyawaki
344 (RIKEN Center for Brain Science) for their kind provision of *App*$^{NL\text{-}F/NL\text{-}F}$ mouse brains; and Drs.
345 Takashi Saito (Nagoya City University) and Takaomi C Saido (RIKEN Center for Brain Science) for
346 sharing *App*$^{NL\text{-}G\text{-}F}$ mice. K.A. is supported by Juntendo Specialized Training for Aspiring Researchers
347 (J-STAR) program at Juntendo University School of Medicine.

References

1. Scheltens P, De Strooper B, Kivipelto M, Holstege H, Chetelat G, Teunissen CE, et al. Alzheimer's disease. Lancet. 2021;397(10284):1577-90.

2. Chen GF, Xu TH, Yan Y, Zhou YR, Jiang Y, Melcher K, et al. Amyloid beta: structure, biology and structure-based therapeutic development. Acta Pharmacol Sin. 2017;38(9):1205-35.

3. Hampel H, Hardy J, Blennow K, Chen C, Perry G, Kim SH, et al. The Amyloid-beta Pathway in Alzheimer's Disease. Mol Psychiatry. 2021;26(10):5481-503.

4. Hunter S, Brayne C. Understanding the roles of mutations in the amyloid precursor protein in Alzheimer disease. Mol Psychiatry. 2018;23(1):81-93.

5. Long JM, Holtzman DM. Alzheimer Disease: An Update on Pathobiology and Treatment Strategies. Cell. 2019;179(2):312-39.

6. Hardy JA, Higgins GA. Alzheimer's disease: the amyloid cascade hypothesis. Science. 1992;256(5054):184-5.

7. Selkoe DJ, Hardy J. The amyloid hypothesis of Alzheimer's disease at 25 years. EMBO Mol Med. 2016;8(6):595-608.

8. Jucker M, Walker LC. Alzheimer's disease: From immunotherapy to immunoprevention. Cell. 2023;186(20):4260-70.

9. DeTure MA, Dickson DW. The neuropathological diagnosis of Alzheimer's disease. Mol Neurodegener. 2019;14(1):32.

367 10. Thal DR, Rub U, Orantes M, Braak H. Phases of A beta-deposition in the human brain and
368 its relevance for the development of AD. Neurology. 2002;58(12):1791-800.
369 11. Masters CL, Multhaup G, Simms G, Pottgiesser J, Martins RN, Beyreuther K. Neuronal origin
370 of a cerebral amyloid: neurofibrillary tangles of Alzheimer's disease contain the same protein as the
371 amyloid of plaque cores and blood vessels. EMBO J. 1985;4(11):2757-63.
372 12. Wong CW, Quaranta V, Glenner GG. Neuritic plaques and cerebrovascular amyloid in
373 Alzheimer disease are antigenically related. Proc Natl Acad Sci U S A. 1985;82(24):8729-32.
374 13. Iwatsubo T, Odaka A, Suzuki N, Mizusawa H, Nukina N, Ihara Y. Visualization of A beta
375 42(43) and A beta 40 in senile plaques with end-specific A beta monoclonals: evidence that an initially
376 deposited species is A beta 42(43). Neuron. 1994;13(1):45-53.
377 14. Murphy GM, Jr., Forno LS, Higgins L, Scardina JM, Eng LF, Cordell B. Development of a
378 monoclonal antibody specific for the COOH-terminal of beta-amyloid 1-42 and its
379 immunohistochemical reactivity in Alzheimer's disease and related disorders. Am J Pathol.
380 1994;144(5):1082-8.
381 15. Yang F, Mak K, Vinters HV, Frautschy SA, Cole GM. Monoclonal antibody to the C-
382 terminus of beta-amyloid. Neuroreport. 1994;5(16):2117-20.
383 16. Saido TC, Iwatsubo T, Mann DM, Shimada H, Ihara Y, Kawashima S. Dominant and
384 differential deposition of distinct beta-amyloid peptide species, A beta N3(pE), in senile plaques.
385 Neuron. 1995;14(2):457-66.

386 17. Saito T, Matsuba Y, Mihira N, Takano J, Nilsson P, Itohara S, et al. Single App knock-in
387 mouse models of Alzheimer's disease. Nat Neurosci. 2014;17(5):661-3.
388 18. Okamoto S, Yamauchi K, Sohn J, Takahashi M, Ishida Y, Furuta T, et al. Exclusive labeling
389 of direct and indirect pathway neurons in the mouse neostriatum by an adeno-associated virus vector
390 with Cre/lox system. STAR Protoc. 2021;2(1):100230.
391 19. Yamauchi K, Okamoto S, Ishida Y, Konno K, Hoshino K, Furuta T, et al. Fluorochromized
392 tyramide-glucose oxidase as a multiplex fluorescent tyramide signal amplification system for
393 histochemical analysis. Sci Rep. 2022;12(1):14807.
394 20. Schneider CA, Rasband WS, Eliceiri KW. NIH Image to ImageJ: 25 years of image analysis.
395 Nat Methods. 2012;9(7):671-5.
396 21. Kim KS, Wen GY, Bancher C, Chen CMJ, Sapienza VJ, Hong H, et al. Detection and
397 Quantitation of Amyloid B-Peptide with 2 Monoclonal-Antibodies. Neuroscience Research
398 Communications. 1990;7(2):113-22.
399 22. Horikoshi Y, Sakaguchi G, Becker AG, Gray AJ, Duff K, Aisen PS, et al. Development of
400 Abeta terminal end-specific antibodies and sensitive ELISA for Abeta variant. Biochem Biophys Res
401 Commun. 2004;319(3):733-7.
402 23. Sato K, Higuchi M, Iwata N, Saido TC, Sasamoto K. Fluoro-substituted and 13C-labeled
403 styrylbenzene derivatives for detecting brain amyloid plaques. Eur J Med Chem. 2004;39(7):573-8.
404 24. Sasaguri H, Hashimoto S, Watamura N, Sato K, Takamura R, Nagata K, et al. Recent

405 Advances in the Modeling of Alzheimer's Disease. Front Neurosci. 2022;16:807473.

406 25. Sasaguri H, Nilsson P, Hashimoto S, Nagata K, Saito T, De Strooper B, et al. APP mouse

407 models for Alzheimer's disease preclinical studies. EMBO J. 2017;36(17):2473-87.

408 26. Yang Y, Arseni D, Zhang W, Huang M, Lovestam S, Schweighauser M, et al. Cryo-EM

409 structures of amyloid-beta 42 filaments from human brains. Science. 2022;375(6577):167-72.

410 # Supporting information

411 **S1 table. Primary Abs used in this study.**

412 **S2 table. Secondary Abs used in this study**

Fig. 1

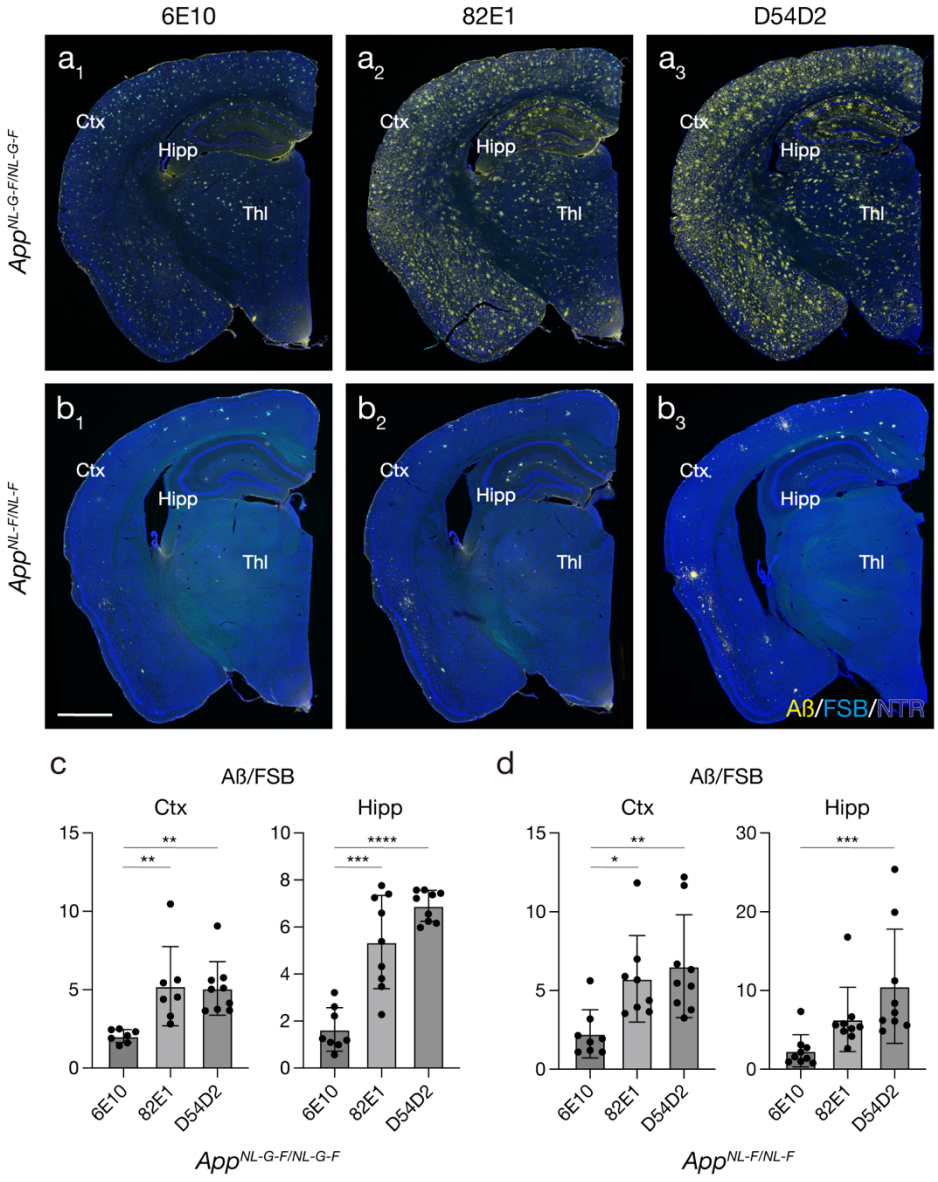
6E10
82E1
D54D2
a1
a2
a3
b1
b2
b3
Ctx
Hipp
Thl
AßFSBNTR
AppNL-G-F/NL-G-F
AppNL-F/NL-F
c
d
Aß/FSB
Ctx
Hipp
6E10
82E1
D54D2
AppNL-G-F/NL-G-F
AppNL-F/NL-F

Fig. 2

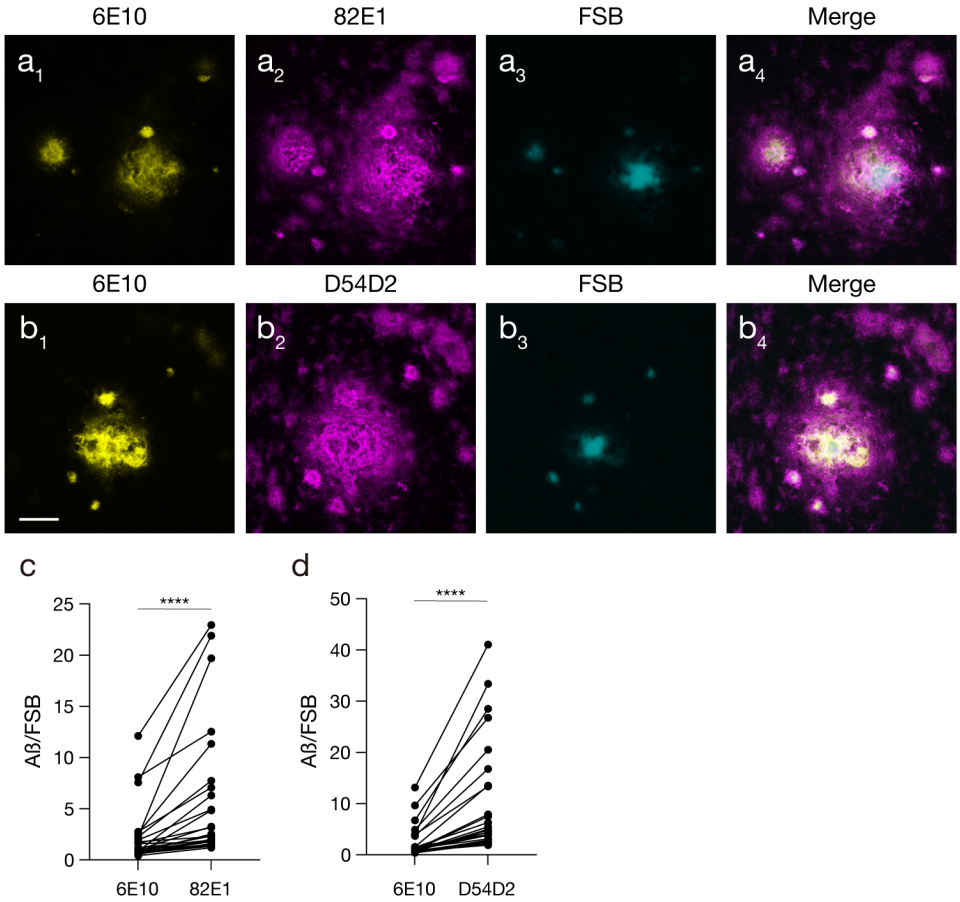
6E10
82E1
FSB
Merge
a1
a2
a3
a4
6E10
D54D2
FSB
Merge
b1
b2
b3
b4
c
Aß/FSB
25
20
15
10
5
0
****
6E10
82E1
d
Aß/FSB
50
40
30
20
10
0
****
6E10
D54D2

Fig. 3

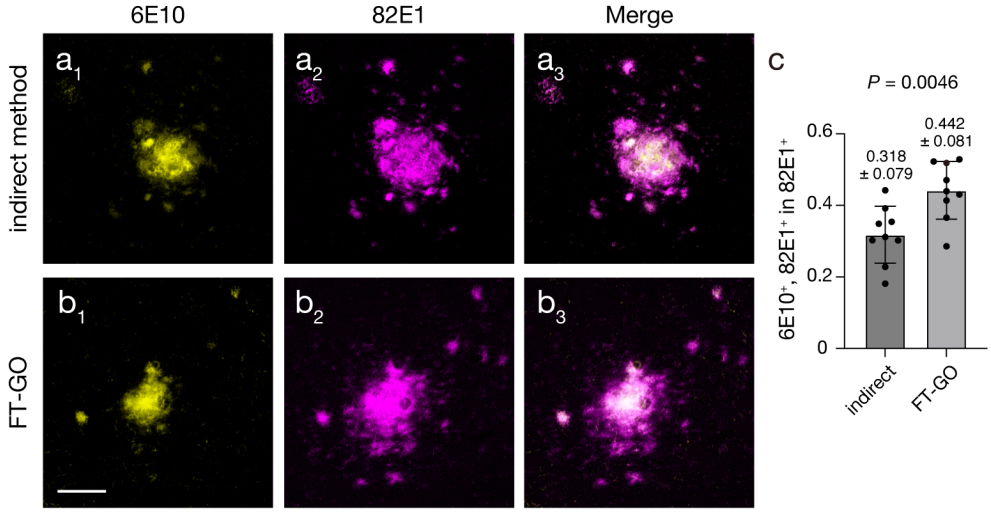
6E10
82E1
Merge
indirect method
FT-GO
a1
a2
a3
b1
b2
b3
c
P = 0.0046
0.318
± 0.079
0.442
± 0.081
6E10+, 82E1+ in 82E1+
0.6
0.4
0.2
0
indirect
FT-GO

Fig. 4

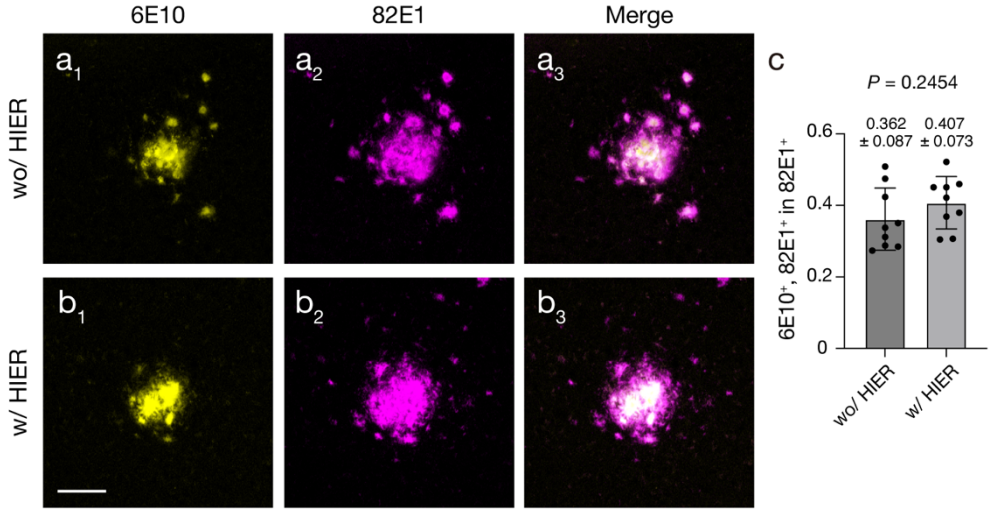
6E10
82E1
Merge
wo/ HIER
w/ HIER
a1
a2
a3
b1
b2
b3
c
P = 0.2454
0.362 ± 0.087
0.407 ± 0.073
6E10+, 82E1+ in 82E1+
0.6
0.4
0.2
0
wo/ HIER
w/ HIER